Journal of Inclusion Phenomena and Molecular Recognition in Chemistry **14**: 327–337, 1992.

Formation of Polypyrrole Chains in Alumina and Chromia-Pillared Layered Phosphates

PEDRO MAIRELES-TORRES, PASCUAL OLIVERA-PASTOR, ENRIQUE RODRÍGUEZ CASTELLÓN, and ANTONIO JIMÉNEZ LÓPEZ
Departamento de Química Inorgánica, Universidad de Málaga, Apdo. 59, Málaga, Spain

ANTHONY A. G. TOMLINSON
ITSE, Rome Research Area C.N.R., Rome, Italy

(Received 17 June 1992; in final form: 4 December 1992)

Abstract. The reaction of gaseous pyrrole (pyr) with Cu^{2+} exchanged alumina- and chromia-pillared α-tin and α-zirconium phosphates has been investigated. Preliminary exchange with Cu^{2+} reveals differences in ordering in the two types of oxide-pillared materials, ascribed to differences in precursor insertion during their preparation. In both oxide-pillared types, the pyr rapidly polymerises in the pores (not on the surface). Optical spectra and XPS evidence point to the presence of more than one type of pyr polymer, and hence of a porous system. The optical properties are typical of mixed neutral and bipolaron states with the presence of low-oxidation level polypyrrole. Based on similarities in optical properties with zeolite analogues, it is suggested that the starting materials contain porous systems similar to both zeolite-Y and mordenite present together. As for zeolite-Y and mordenite analogues, the materials have negligible conductances ($<10^{-9}\,\Omega^{-1}\,cm^{-1}$), which is ascribed to the presence of only short polymeric pyr units.

Key words. Polypyrrole, alumina, chromia, pillaring, phosphates.

1. Introduction

Polymerising N- and S-containing organics *in situ* in layered and cavity materials gives rise to conducting polymer composites in which the conductance properties depend crucially on the available cavity (size, acidity, etc.). For example, polymerising pyrrole *in situ* in simple layered materials, such as FeOCl and V_2O_5, gives rise to chain-branched, conducting hybrids [1], whereas the constraints present in a zeotype, such as $[(Me_3Sn)_3Fe(CN)_6]$, leads to non-chain-branched polymer hybrids [2]. In the limit of a very constrainted environment, only small segments of the polymer are produced, providing 'molecular-wire' nanocomposites, as recently reported by Bein *et al.* [3] for polypyrrole (Ppy) inside zeolite Y and mordenite. These authors suggested that the polymerisation was 'directed' by the restricted space available in the zeolite, leading to cutting of the Ppyr 'wires' and hence a nonconducting character. Further, these authors found that polymerisation did not occur in zeolite A, because of channel-exclusion to incoming pyrrole.

The uptake and polymerisation of small molecules such as pyrrole (kinetic size 5.7 Å) thus provides a probe of pore accessibility, geometry and acidity in porous materials. There have been recent advances in preparing porous alumina- and chromia-pillared phosphates [4] (i.e. layered materials in which the layers are propped apart by oxide nanoparticles) [5]. However, little is yet known as regards

the channel and pore structure of such materials. In addition, since oxide-pillared materials have acidities and porosities different from zeolites, the molecular wires eventually formed would also be expected to differ from those in zeolites.

With this in mind, we have investigated the interaction between pyrrole (pyr) and a series of the above materials (exchanged with Cu^{2+}, to permit oxidative polymerisation) chosen to provide a range of pore sizes. Polymerisation occurs inside the cavities, and there is evidence for the presence of pores similar to that in mordenite (6.7 × 8 Å pore channel opening) and zeolite Y (7.5 Å pore diameter).

2. Experimental

2.1. MATERIALS

α-Tin [$Sn(HPO_4)_2 \cdot H_2O$] and α-zirconium [$Zr(HPO_4)_2 \cdot H_2O$] phosphates were chosen as the host matrices. Two kinds of aluminium solution were employed to prepare the aluminium oligomer–phosphate intercalates: a partially neutralized $AlCl_3$ solution with NaOH (OH/Al = 2), in which the major species is the tridecameric ion $[Al_{13}O_4(OH)_{24}(H_2O)_{12}]^{7+}$; and a solution of the commercial product Chlorhydrol (Reheis Co.). The chromium oligomer– phosphate intercalates were obtained by *in situ* polymerisation of Cr^{3+} acetate solutions in the presence of the phosphate. All intercalation compounds were then calcined at 400°C. Details of the preparation and characterisation have been described previously [4].

Three differing sets of starting materials were used: (i) alumina-pillared tin phosphates designated Al_{13}–SnP and chlor–SnP, having free heights of 5.8 and 6.5 Å, respectively, and possessing wide pore-size distributions; (ii) the chromia-pillared tin phosphates designated Cr-SnP-2, -4 and -7, having similar free heights (7.5, 7.4 and 7.3 Å, respectively), BET surface areas of 267, 312 and 249 m^2g^{-1} and narrow pore-size distributions (r_p = 8-20 Å); and (iii) the zirconium analogues of (ii): Cr-ZrP-5, with the narrowest pore size distribution of that series [4].

Pyrrole was a commercial product (Aldrich, 99%) and was used as received. Bulk Ppyr for comparison purposes was prepared by standard methods [6], i.e. the oxidation of pyrrole with $FeCl_3$ (Aldrich).

2.2. PREPARATION

In preliminary experiments, the presence of water as solvent was found to be unfavourable for intrapore polymerisation, leading to the lowest polymer yields (as judged from TG results). Test runs were also carried out in the presence or absence of air; no differences in the materials were found under the two conditions.

Each host material was first completely exchanged [4] with Cu^{2+}, evacuated (10^{-4} torr, at 523 K) and then gaseous pyrrole diffused for 24h at 333 K *in vacuo*. The colour changes immediately from white (Al_2O_3-pillared materials) or dirty-green (Cr_2O_3-pillared materials) to blue-black of different hues. Any excess pyrrole was removed under vacuum (10^{-3} torr, 3 h). Analyses of final materials are shown in Table I. The BET surface area of each material was measured after exchange with Cu^{2+} and after reaction with pyrrole. Textural characteristics are listed in Table II. In one experiment, with Cr-ZrP-5, the Cu^{2+}-exchange step was neglected.

Table I. Chemical composition of Cu^{2+}-exchanged pillared materials containing Ppyr[a]

Starting material	Al_2O_3 or Cr_2O_3 (%)	Cu (%)	H_2O (%)	C (%)	N (%)
Al_{13}-SnP	21.8	2.0	2.3	7.1	2.1
Chlor-SnP	28.0	8.3	1.5	9.3	2.6
Cr-SnP2	29.7	4.6	4.4	7.9	2.3
Cr-SnP4	30.2	5.6	8.7	7.8	2.4
Cr-SnP7	24.3	7.5	1.5	9.8	2.8
Cr-ZrP5	31.1	6.9	2.2	12.3	3.6
Cr-ZrP5*	32.3	–	2.6	14.9	4.4

Starting material	Empirical formulation
Al_{13}-Snp	$Sn[Al_{2.0}O_{1.9}(OH)_{0.5}](pyr)_{0.7}Cu_{0.15}(PO_4)_2 0.6\ H_2O$[b]
Chlor-SnP	$Sn[Al_{4.0}O_{3.1}(OH)_{5.7}](pyr)_{1.4}Cu_{0.95}(PO_4)_2 0.6\ H_2O$
Cr-SnP2	$Sn(Cr_{2.4}O_{2.5}(OH)_{1.1}](pyr)_{1.0}Cu_{0.45}(PO_4)_2 1.5\ H_2O$
Cr-SnP4	$Sn[Cr_{2.7}O_{3.6}(OH)_{0.1}](pyr)_{1.1}Cu_{0.60}(PO_4)_2 3.3 H_2O$
Cr-SnP7	$Sn[Cr_{1.9}O_{1.9}(OH)_{1.3}](pyr)_{1.2}Cu_{0.70}(PO_4)_2 0.5\ H_2O$
Cr-ZrP5	$Zr[Cr_{3.0}O_{2.5}(OH)_{3.6}](pyr)_{1.9}Cu_{0.8}(PO_4)_2 0.9\ H_2O$
Cr-ZrP5*	$Zr[Cr_{3.0}O_{2.5}(OH)_{3.6}](pyr)_{2.2}H_{1.6}(PO_4)_2 1.0\ H_2O$

[a] From chemical, thermal and CNH analyses.
[b] Species in brackets are the metal oxyhydroxide pillars, formed by calcination of the respective precursors at 400°C.
* No Cu^{2+}.

Table II. Textural characteristics before and after exchange with Cu^{2+}

Sample	S_{BET} ($m^2\ g^{-1}$)	C_{BET}	S_{ac} ($m^2\ g^{-1}$)	V_p ($cm^3\ g^{-1}$)	d_p (Å)†
Al_{13}-SnP	174	11	262	0.379	87
Al_{13}-SnP + Cu^{2+}	84	66	97	0.258	123
Chlor-SnP	190	26	247	0.271	57
Chlor-SnP + Cu^{2+}	101	117	115	0.215	86
Cr-SnP-2	267	99	287	0.247	37
Cr-SnP-2 + Cu^{2+}	211	318	197	0.159	30
Cr-SnP-4	312	313	295	0.209	27
Cr-SnP-4 + Cu^{2+}	201	223	192	0.193	39
Cr-SnP-7	249	29	315	0.310	50
Cr-SnP-7 + Cu^{2+}	175	132	180	0.146	34
Cr-ZrP-5*	388	156	394	0.247	25

† Using the Cranston and Inkley method [8].
* No Cu^{2+}.

2.3. CHARACTERISATION AND PHYSICAL MEASUREMENTS

The amounts of intercalated Ppyr were determined by CHN analysis. Manipulations were followed throughout using powder XRD (Siemens D500 diffractometer; Ni-filtered Cu-K_α radiation), TGA/DTA were performed on a Rigaku instrument

(heating rate 10°C/min). UV/visible spectra were obtained on a Shimadzu UV 3100 and IR spectra were measured on a Perkin Elmer 883 spectrophotometer. Conductances were measured (R.T.) by the standard four-probe de Paul *et al.* technique [7]. All the materials were found to be non-conductors (i.e. $\sigma < 10^{-9}$ S).

Adsorption–desorption measurements were carried out on a conventional volumetric apparatus. Samples were first degassed at 473 K overnight and adsorption–desorption of N_2 followed at 77.4 K.

X-ray photoelectron spectra were recorded on a VG ESCA 3 Mk II instrument using Al $K_{\alpha 1,2}$ ($h\nu$ = 1486.6 eV) as the exciting source at a constant power of 280 W (12 kV, 20 mA). The equipment was interfaced to a data system which allowed accumulation of spectra. The C_{1s} peak at 284.4 eV was used as calibration standard.

3. Results and Discussion

We first examine the porosity data on the starting Cu^{2+}-exchanged materials, which provide some insight into the nature of the starting materials. In all cases, exchange with Cu^{2+} causes marked decreases in the surface area: by 60–80 m^2g^{-1} for the chromia-pillared cases, and to less than half in Al_{13}-SnP and chlor-SnP (see Table II). Secondly, the pore size distributions also behave very differently between the two types of oxide pillar. The pore distribution in the alumina-containing materials is destroyed, to give rise to wider distributions centred at higher pore sizes (see Figure 1). In Al_{13}-SnP the mesopores distribution is centred at ca. 50 Å, and in Chlor-SnP at about 25 Å (closer to the original one). These large changes suggest that the Cu^{2+} has exchanged on cut layers, to provoke an inhomogeneous reordering of the layer packets, as illustrated in Scheme 1. Much (or even most) porosity

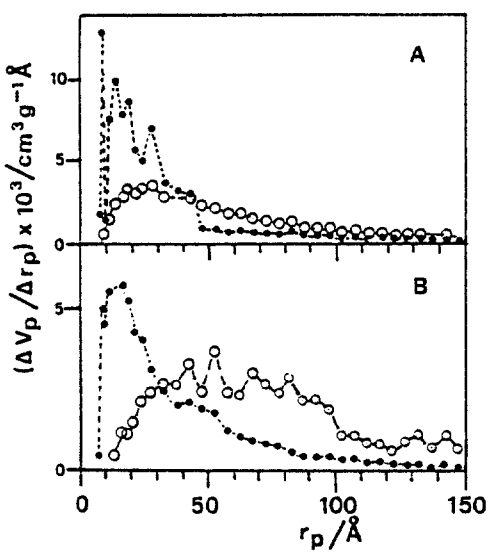

Fig. 1. Pore size distributions. (A) Al_{13}-SnP, (B) Chlor-SnP before (●) and after (○) exchange with Cu^{2+}. Calculated by the cylindrical pore method of Cranston and Inkley [8], using the data of the N_2 adsorption branch.

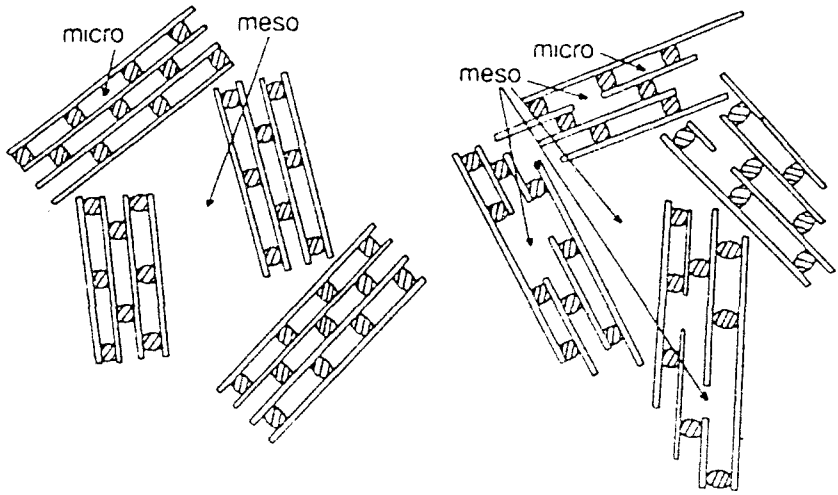

Scheme 1

in this material may then be due to the interstices between close-packed layers. (Curiously, the XRD of the Cu^{2+}-exchanged alumina-pillared compounds do not undergo particular changes).

Porosity changes in the chromia series are less drastic; exchange still leaves a narrow, but different pore distribution. In addition, and allowing for the well-known deficiences of the BET method, it appears that Cu^{2+} exchanges preferentially into the larger mesopores in Cr-SnP-2 and Cr-SnP-7, but into the smaller ones in Cr-SnP-4 (Figure 2).

The starting alumina-pillared materials were prepared by intercalation of aluminium hydroxyoxo-cations into the layered phosphates, whereas the chromia-pillared ones were obtained via a forced hydrolysis of $Cr(OAc)_3$. The results also suggest that there are specific sites for Cu^{2+}, because not all the internal surface is exchanged, despite the fact that the maximum loading was used.

Turning to the interaction of the materials with pyrrole, the chemical analyses of Table I confirm high loadings, showing that polymerisation is not simply superficial and visual inspection of SEM micrographs confirm that the polymer is not deposited on external surfaces. Secondly, in all cases the basal spacings do not change on reaction with pyrrole, and the host crystallinity is not significantly reduced. Finally, maximum loadings were achieved after only short times (1 h), which may be contrasted with FeOCl which requires days to go to completion [1] and zeolite Y and mordenite, which require hours [3]. These results all point to the presence of accessible internal surfaces in both types of host, which remain pillared after reaction. In agreement with this conclusion the IR spectra are similar to those in bulk Ppyr [9]. However, there are small changes in the IR spectra with the host matrix in the C—C and C—H ring vibration region; e.g. for Cr-SnP-2/Ppyr the characteristic band lies at 1560 cm^{-1} (1540 cm^{-1} in bulk Ppy), which we, with Bein *et al.* [3], also ascribe to differences in the pore electrostatic environment. The absence of skeletal vibrations in the 1241–1408 cm^{-1} region, is instead probably due to damping of these modes because of the restricted space available.

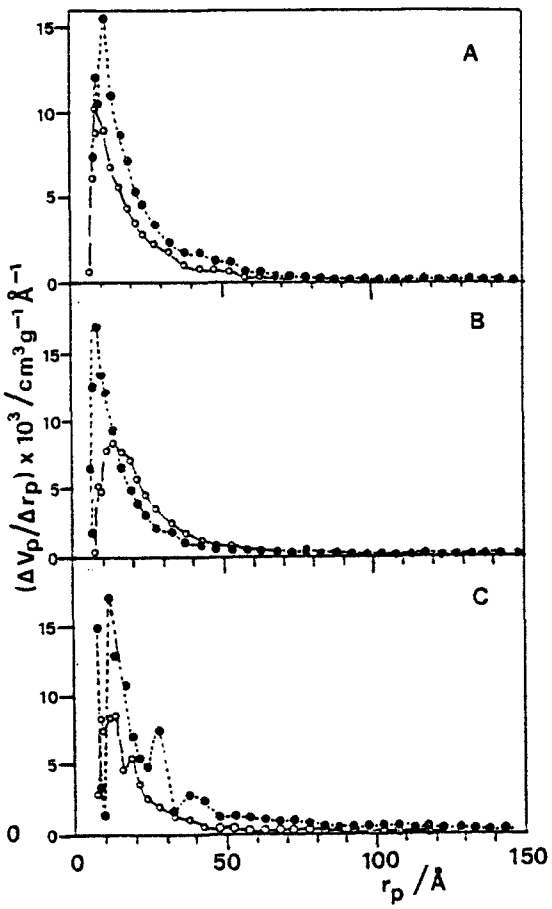

Fig. 2. Pore size distributions before (●) and after (○) exchange with Cu^{2+}. A) Cr-SnP-2, B) Cr-SnP-4, C) Cr-SnP-7. Details as for Fig. 1.

Ppyr loadings are high, e.g. Cu^{2+}-exchanged CrSnP-4 contains a maximum of 3.13 mmole pyr/g. matrix. This value can be compared with values of 3.17 in FeOCl [1], 0.24 in mordenite [3] and 3.84 in zeolite Y [3]. (According to the literature [10], the optimal oxidant: pyrrole ratio is 2.46.) The chlor-SnP material giving almost twice the loading of Al_{13}-SnP. A possible explanation is that the break-up caused by exchange leaves more internal, structured pillared spaces in the former than in the latter. (This result also confirms that polymerisation is not superficial.) Finally, further confirmation that pyrrole has polymerised in the pores is provided by the fact that all the final solids were non-porous (BET surface areas in the range 5–20 m^2g^{-1}). This implies that all (or most) of the remaining available internal surfaces have been covered by the Ppy.

The results for Cr-Zr-P5* provide a clinching argument. The reaction with pyr was carried out with this material as prepared, i.e. without prior Cu^{2+} exchange, yet it also gives polymerisation, which suggests that the chromia pillar itself is

responsible for the oxidative polymerisation (and by itself can generate carbocations). Although it was not possible to detect chromium oxidation states higher than III by XPS analysis, the presence of some chromium species with high oxidation states in chromia-pillared phosphates has been suggested by the appearance of a very-low-energy broad band in the near-IR region [4]. Indeed, it takes up the most Ppyr (see Table I), and we ascribe this to the fact that there is no blocking of surfaces by Cu^{2+} ions in this case.

All composites are thermally quite stable. A typical TG-DTA curve is shown in Figure 3. The composites are anhydrous (no endotherms are observed at low temperature). The very intense exotherm centred at 360°C is attributed to the combustion of Ppyr which is completely lost at 400°C.

Neutral Ppyr gives an optical spectrum with a broad absorption at 1.2 eV, and a much higher intensity band [11] at 3 eV. At lower oxidation levels, they both shift to lower energy; highly doped electrolytically produced Ppyr giving bands at 0.7 and 2.3 eV, attributable to bipolarons [9]. Using this as a guide, together with the

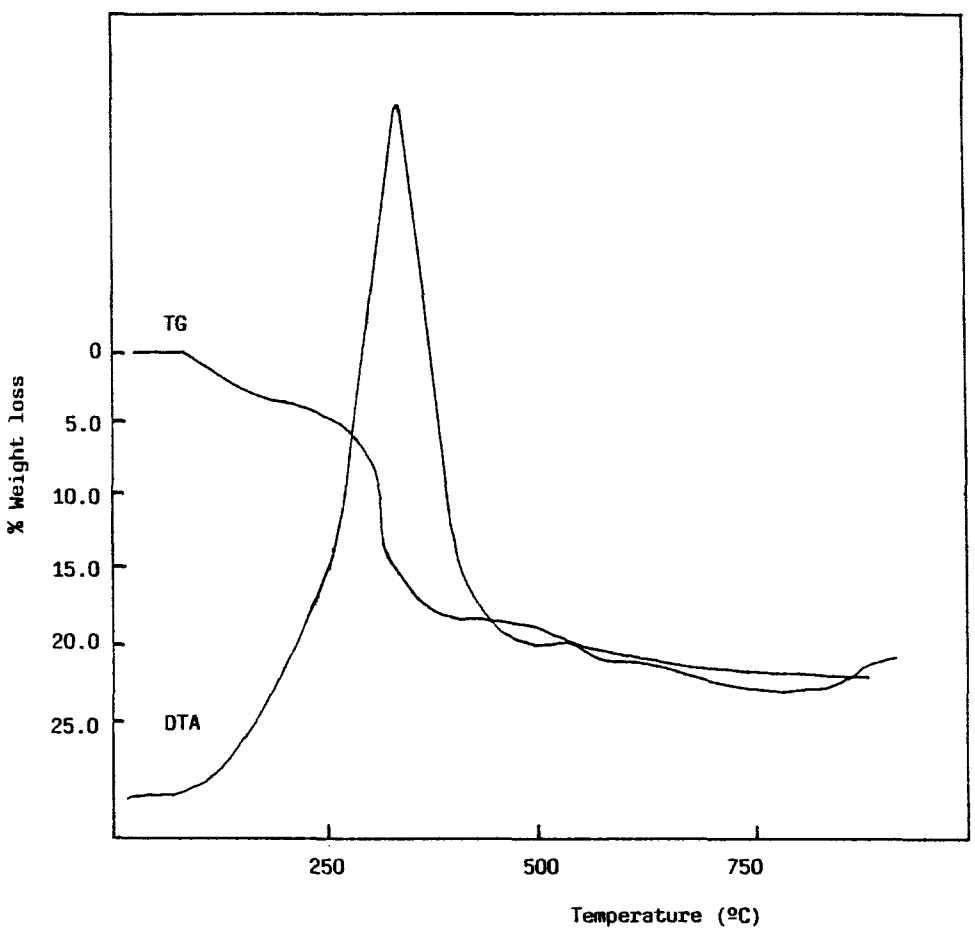

Fig. 3. Typical TG/DTA Analysis of a CrSnP-pyr material.

standard scheme for pyr oxidation [9], Bein *et al.* [3] suggested that bipolarons (spinless dications associated with quinoid structures over four to five rings) were present in zeolite Y and in mordenite.

The optical spectra in the pillared matrices do not show such clearly separated features, because intense overlapped bands appear in the vis/near IR region, (see Figure 4). Apart from demonstrating that more than one polymer is present, there are some indications as to the species involved. The two transitions, at 1.2 eV and 0.75 eV in the alumina-pillared materials suggest that both a neutral Ppyr and a bipolaron Ppyr are present simultaneously.

Band resolution is a little clearer in the chromia matrices (although again Cr^{3+} $d-d$ bands hinder the interpretation). In the CrZrP-5-Ppyr sample (without Cu^{2+}) two features are observed at 1.97 and 2.69 eV, (Figure 5) indicating the presence of bipolarons. In the spectrum of the same composite with Cu^{2+} a higher number of bands are present, which is indicative of the presence of neutral and bipolaron Ppyr at different oxidation levels. Further, the band positions imply that the starting materials contain both mordenite-like and zeolite-Y-like porosity.

The XPS spectra confirm that two (and not more) species are present. All materials show N (ls) bands at 400.05 ($\pm$0.1) eV and 398.5 ($\pm$0.2) eV (Figure 6). The latter is assignable to a neutral nitrogen and the former to a charged nitrogen. The area ratio between the two (Table III) changes throughout the two series; interestingly, in Cr-Zr-P5* the neutral polymer is present predominantly, as compared with the charged one(s). Further, there are changes in the uncharged/charged N ratio on X-ray irradiation. This indicates that complex Cu^{2+}–Cu^{+}-polymer interactions occur. These are under investigation.

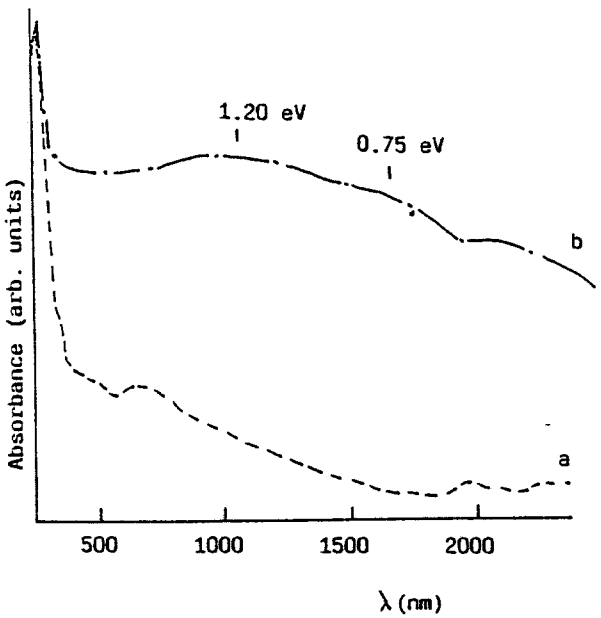

Fig. 4. Optical spectra of Al_{13}-SnP (a), after Cu^{2+}-exchange, and after pyr polymerisation (b).

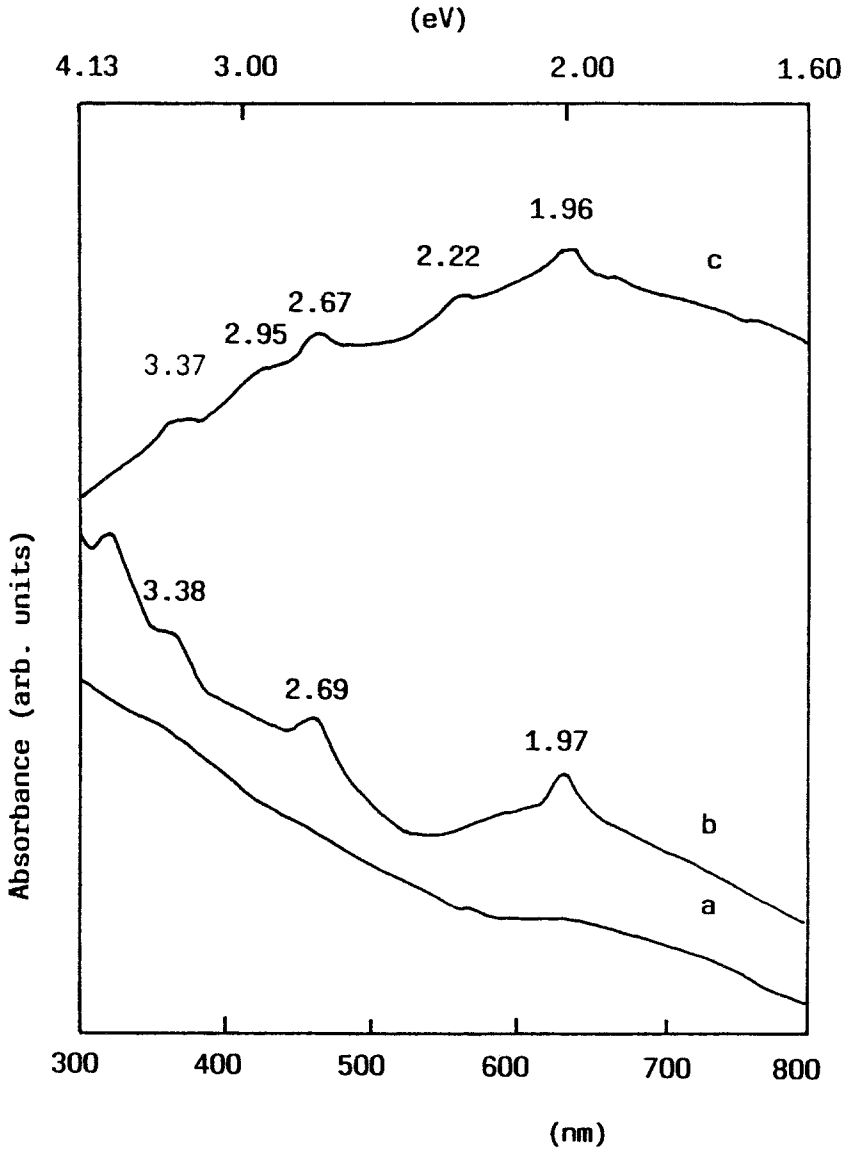

Fig. 5. Optical spectra of Cr-ZrP-5 materials: (a) pillared matrix Cr-ZrP–5, (b) material (a) containing polymerized pyrrole, (c) Cu^{2+}-exchanged material (a) containing polymerized pyrrole.

In conclusion, both alumina and chromia-pillared layered phosphates can generate the carbocations necessary for allowing polymerisation of pyrrole within their pores. Their internal surfaces are more accessible than zeolites, but also give rise to non-conducting polymers. More detailed studies of pore access and oligomer molecular wire location will require completion of experiments on more uniform alumina-pillared analogues [12].

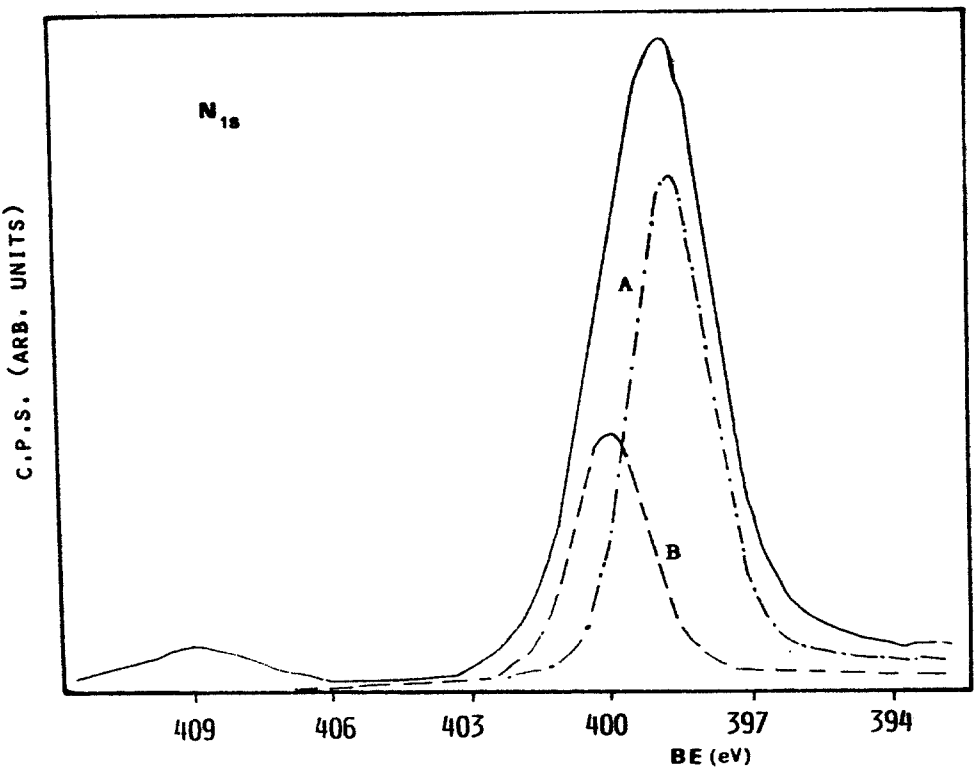

Fig. 6. XPS spectrum of Cu^{2+}-exchanged Cr-ZrP-5 containing Ppyr.

Table III. XPS spectra of materials

Material	*N*1*s* (A)	*N*1*s* (B)	Area A/Area B	Area A/Area B after 2 h irradiation
Ppyr/Al_{13}SnP	398.56	400.17	3.61	3.92
Ppyr/Chlor-SnP	398.89	400.29	2.01	–
Ppyr/Cr-SnP-4	398.76	400.15	2.39	2.62
Ppyr/Cr-SnP-7	398.57	400.06	3.61	2.64
Ppyr/CrZrP-5	398.70	400.14	5.72	3.38
Ppyr/Cr-ZrP-5*	398.30	400.02	10.10	6.64

* No Cu^{2+}

Acknowledgements

We thank CICYT (Spain) Project MAT-90-298 for financial support and A.A.G.T. thanks the Spanish Ministry of Education for a Visiting Professorship, during which time this work was completed.

References

1. M. G. Kanatzidis, L. M. Tonge, T. J. Marks, H. O. Marcy and C. R. Kanewurf: *J. Am. Chem. Soc.* **109**, 3797 (1987); H. G. Kanadtzidis, C.-G. Wu, H. O. Marcy, and C. R. Kannewurf: *J. Am. Chem. Soc.* **111**, 4139 (1989); H. Inoue, H. Yoneyama: *J. Electroanal. Chem. Interfacial Electrochem.* **233**, 291 (1987).
2. P. Brandt, R. D. Fischer, E. Sánchez Martínez, and R. Díaz Calleja: *Angew. Chem., Int. Ed. Engl.* **28**, 1265 (1989).
3. T. Bein and P. Enzel: *Angew. Chem., Int. Ed. Engl.* **28**, 1692 (1989); T. Bein, in *Electron Transfer in Biology and the Solid State*, ACS Series, 1991.
4. P. Maireles-Torres, P. Olivera-Pastor, E. Rodríguez-Castellón, A. Jiménez-López, and A. A. G. Tomlinson: *J. Solid State Chem.* **94**, 368 (1991); *ibid*: *J. Mat. Chem.* **1** (3), 319 (1991); *ibid*: *J. Mat. Chem.* **1** (5), 739 (1991).
5. A. A. G. Tomlinson, in *Pillared Layered Structures. Current Trends and Applications*, ed. I. V. Mitchell, Elsevier Applied Science, London, 1990; R. Burch: *Catalysis Today* **2** (2–3), 185 (1988); R. M. Barrer, *Zeolites and Clay Minerals as Sorbents and Molecular Sieves*, Academic, London, 1978; S. Cheng, G. Z. Peng and A. Clearfield: *I & EC Prod. Res. Develop.* **23**, 219 (1984).
6. R. E. Myers: *J. Electron. Mat.* **15**, 61 (1986).
7. E. W. Paul, A. J. Ricco and M. S. Wrighton: *J. Phys. Chem.* **89**, 1441 (1985).
8. R. W. Cranston and F. A. Inkley: *Adv. Catal.* **9**, 143 (1957).
9. G. B. Street, in *Handbook of Conducting Polymers*, ed. T. A. Skotheim, Marcel Dekker, New York, 1986, Vol. 1, p. 265.
10. S. P. Armes: *Synth. Met.* **20**, 365 (1987).
11. G. B. Street, T. C. Clarke, M. Krounbi, K. K. Kanazawa, V. Lee, P. Pfluger, J. C. Scott and G. Weiser: *Mol. Cryst. Liq. Cryst.* **83**, 253 (1982).
12. P. Maireles-Torres, P. Olivera-Pastor, E. Rodríguez-Castellón, A. Jiménez-López, and A. A. G. Tomlinson: in preparation.